International Journal of Heat and Fluid Flow 30 (2009) 462–470

Contents lists available at ScienceDirect

International Journal of Heat and Fluid Flow

journal homepage: www.elsevier.com/locate/ijhff

Lagrangian particle dispersion in turbulent flow over a wall mounted obstacle

D.G.E. Grigoriadis [a,*], S.C. Kassinos [a]

[a] Computational Sciences Laboratory UCY-CompSci, University of Cyprus, 75 Kallipoleos Avenue, P.O. Box 20537 Nicosia 1678, Cyprus

ARTICLE INFO

Article history:
Received 30 September 2008
Received in revised form 31 December 2008
Accepted 10 January 2009
Available online 24 February 2009

Keywords:
Incompressible flow
Large-eddy simulation
Immersed boundary method
Particle dispersion
Wake flow

ABSTRACT

Large-eddy simulations (LES) of particle-laden turbulent flows are presented in order to investigate the effects of particle response time on the dispersion patterns of a space developing flow with an obstruction, where solid particles are injected inside the wake of an obstacle [Vincont, J.Y., Simoens, S., Ayrault M., Wallace, J.M., 2000. Passive scalar dispersion in a turbulent boundary layer from a line source at the wall and downstream of an obstacle. J. Fluid Mech. 424, 127–167]. The numerical method is based on a fully explicit fractional step approach and finite-differences on Cartesian grids, using the immersed boundary method (IBM) to represent the existence of solid obstacles. Two different turbulence models have been tested, the classical Smagorinsky turbulence model and the filtered structure function model. The dispersed phase was modelled either by an Eulerian approach or a Lagrangian particle tracking scheme of solid particles with Stokes numbers in the range $St = 0$–25, assuming one-way coupling between the two phases. A very good agreement was observed between the Lagrangian and Eulerian approaches. The effect of particle size was found to significantly differentiate the dispersion pattern for the inhomogeneous flow over the obstacle. Although in homogeneous flows like particle-laden turbulent channels near-wall particle clustering increases monotonically with particle size, for the examined flow over an obstacle, preferential concentration effects were stronger only for an intermediate range of Stokes numbers.

1. Introduction

LES is considered nowadays as a powerful technique for the accurate simulation of turbulent flows. In the last decade, LES has been also successfully applied for the simulation of two-phase flows, which are of great importance in a variety of industrial and environmental applications. Particle-laden flows are typical examples of such multiphase flows, where the particles are simulated with varying degrees of complexity, from simple tracers that are transported by the main flow, to inertial particles that might affect the flow field, diffuse, conglomerate, collide inelastically, etc. LES offers an excellent frame of reference for the modelling of such dispersion phenomena, since it provides instantaneous and time accurate information – at least – for the largest scales of motion.

Several advantages exist when one performs LES-based numerical dispersion studies. First of all a wider range of particle size can be analyzed, and monochromatic (or monodisperse) particles can be considered in order to study in detail the effect of particle size on the dispersion pattern. Secondly, since the instantaneous flow field is available, one can directly examine and establish correlations between the interactions of coherent flow structures and particle motion. This interaction is primarily dominated and determined by inertia effects because particles of different size will selectively interact with different scales of fluid motion. It is therefore expected that the dispersion pattern will heavily depend on particle mass and size. Although the statistical characteristics of dispersion are dominated by well-resolved large scale flow structures (Armenio et al., 1999), the particle's time of response is expected to play an important role on the produced dispersion pattern.

The relative importance of the involved time scales is usually expressed by the characteristic dimensionless Stokes number St defined as the ratio $St = \tau_p/\tau_f$, where τ_f is the characteristic time scale of the fluid phase and τ_p is the particle's relaxation time,

$$\tau_p = \frac{d_p^2 \rho_p}{18\mu_f}, \tag{1}$$

where μ_f if the fluid viscosity and the subscripts (f) and (p) denote the fluid phase and particles, respectively.

In the present study, we focus on the dispersion characteristics of particle-laden inhomogeneous flows for a wide range of St numbers, which – in contrast to homogeneous flow cases – have not been studied extensively. The main objectives were to (i) investigate the potential of the method for inhomogeneous flows typically appearing in environmental applications and (ii) study the dispersion characteristics and preferential concentration effects

* Corresponding author. Tel.: +357 22892296; fax: +357 22892254.
E-mail addresses: grigoria@ucy.ac.cy, dimokratis@hotmail.com (D.G.E. Grigoriadis).

0142-727X/$ - see front matter © 2009 Elsevier Inc. All rights reserved.
doi:10.1016/j.ijheatfluidflow.2009.01.010

in inhomogeneous flows. An Eulerian approach is adopted for the carrier fluid phase, combined with a Lagrangian tracking procedure of solid particles for the dispersed phase. Detailed comparisons with a classical Eulerian approach for both phases are presented and discussed.

In the following sections, the theoretical considerations for the two phases are first presented in Section 2. The validation of the numerical methodology (Section 3) for a particle-laden turbulent channel flow is presented in (Section 4.1). Finally, results from the dispersion analysis in the wake of a wall-mounted obstacle are given in (Section 4.2).

2. Theoretical formulation

2.1. Fluid phase

The fluid motion is governed by the continuity equation and the full set of the Navier–Stokes equations for an incompressible fluid which are formulated in a dimensionless form as,

$$\frac{\partial u_i}{\partial t} = 0, \tag{2}$$

$$\frac{\partial u_i}{\partial t} + \frac{\partial u_i u_j}{\partial x_j} = -\frac{\partial p}{\partial x_i} + \frac{1}{Re}\frac{\partial^2 u_i}{\partial x_j \partial x_j} + f_{IB} \tag{3}$$

where Re denotes a relevant Reynolds number for each case. The last term f_{IB} in the *rhs* of Eq. (3) represents the immersed boundary forcing term. This term is specified so that it dynamically mimics the existence of solid, immersed boundaries (for details see Balaras, 2004).

2.2. Particulate phase

The dispersed phase was described by two different methodological approaches, i.e. by an Eulerian or a Lagrangian approach. In the first case, the concentration field was assumed to be continuum and a transport equation governed the evolution of the concentration field. In the second case the dispersed phase consisted of a collection of transported particles where the force exerted on each particle determined its trajectory. Both methods can be beneficial for different classes of dispersion problems. In cases where the time dependent flow field is not available or when chemical reactions take place, an Eulerian approach might be beneficial. On the other hand, the Lagrangian approach comes at a lower numerical cost and offers a wide range of descriptive capabilities for the dispersed phase. Especially in practical applications, the Lagrangian approach can naturally accommodate physical effects like inertia, stationary or moving sources concentrated in space, elastic or inelastic wall-collisions, particle deposition, etc. Therefore, it offers a convenient tool for dispersion investigations in complicated dispersion studies (Li et al., 2006).

In the present study we consider particle-laden turbulent flows where a number of N_p particles are dispersed. The average volume and mass fractions Φ_v and Φ_m occupied by the particles are simply defined as,

$$\Phi_v = \frac{N_p V_p}{V_{f.tot}} = \frac{N_p \pi d_p^3}{6 V_{f.tot}} \quad \text{and} \quad \Phi_m = \frac{\rho_p}{\rho_f}\Phi_v, \tag{4}$$

where V_p is the volume of a single particle and $V_{f.tot}$ the total volume occupied by the fluid and the solid phase. For volume fraction values smaller than $\Phi_v \sim O(10^{-6})$, a dilute suspension is expected and the interaction between the two phases is classified as an *one way coupling interaction* (Elgobashi, 2006). In these cases of dilute suspension, because of the low particle-concentration, momentum exchange is minimized between the two phases, the particle motion does not modify the flow and the effect of particle motion to the carrier fluid phase can be neglected.

The equation of motion of each solid particle is governed in the most general case by Newton's second law of motion according to,

$$m_p \frac{d\mathbf{u_p}}{dt} = F_D + F_L + F_g + F_{am} + F_{Basset} + F_{PD} + F_{sgs}, \tag{5}$$

where m_p is the mass of each particle. Terms on the *rhs* represent contributions from the drag, lift, gravity, added mass, Basset, pressure drag and subgrid scale forces.

The relative importance of each force in Eq. (5) depends mainly on the particle size d_p, and the density ratio ρ_p/ρ_f between the two phases. Armenio and Fiorotto (2001) studied the importance of these forces acting on particles with respect to the density ratio ρ_p/ρ_f. For a turbulent channel flow at $Re_\tau = 175$, Stokes drag was found to be the dominant force for density ratios in the range of O(1) to O(1000). Compared with drag, Basset force was significantly smaller, pressure drag forces were limited for density ratios O(1), while the added mass force was found three orders of magnitude smaller. In all cases, they concluded that the effect of forces other than Stokes drag on particle dispersion was limited to 1%.

Effects of lift force (Wang et al., 1997), and near wall forces (Arcen et al., 2006) on particle deposition and statistics have been extensively studied for a variety of confined turbulent flows. Most of these studies conclude a limited effect of lift, gravity and near-wall forces on the particle motion and the dispersion characteristics in turbulent flows of high density ratios which concerns the present study. The effects of gravity and lift force on vertical channel flow were studied numerically by Marchioli et al. (2007). Although the velocity profiles and deposition coefficients were found to be influenced by gravity, the qualitative behavior of particles was not significantly affected by the inclusion of gravity and lift forces in the particle's equation of motion.

The last term F_{sgs} of Eq. (5) denotes the contribution of subgrid scale effects on the particle's motion. This term is zero for DNS simulations since all the existing scales are resolved, and the velocity field distribution is known for the smallest scales. For LES though, only the filtered velocity field is computed and particles are normally located inside subgrid scale regions which are not explicitly known. Depending on the available numerical resolution of an LES simulation, the introduced subgrid error can be significant for the evolution of the particle's trajectories (Kuerten and Vreman, 2005). This is especially the case for smaller particles (i.e. *St* numbers) which have smaller relaxation times and respond faster to the flow irregularities (Wang et al., 1997). On the other hand, larger particles with more inertia are less sensitive to the flow field fluctuations because they tend to retain their gained momentum for a longer time.

The effect of *sgs* motion on the particle motion has been investigated by Armenio et al. (1999) using filtered DNS data. They reported that particle dispersion was suppressed when filtered field were used, while the effect of *sgs* terms was found to affect as little as 8–20% the dispersion characteristics depending on the grid resolution. These findings were based on tracer particles without inertia, and thus the effect on larger particles and well-resolved simulations is expected to be even weaker. Therefore, in cases where well-resolved large scales dominate the flow, the statistical features of dispersion for larger particles are expected to depend weakly on the *sgs* motions (Marchioli et al., 2006).

For the present study, particles were assumed to be solid, rigid and spherical colliding in a fully elastic manner with the wall boundaries. Since low volume fractions Φ_v (or concentrations) are considered, the effect of particles on the fluid phase was neglected and particle-particle interactions were not taken into account i.e. *one way coupling* was assumed between the two phases. Due to the density ratio and the size of the released particles, only the drag force was considered to contribute to their equation of motion. Particle lift, buoyancy, Basset and added mass

forces were thus neglected for the present analysis. The effect of gravity would be expected to play an important role only when larger particles are considered by generating a tendency for particle accumulation at the lower walls. In order to isolate such an effect, gravity effects were thus also neglected.

Under these assumptions, the trajectory of each particle located instantaneously at $\mathbf{x_p}$, travelling with velocity $\mathbf{x_p}$ can be computed from,

$$\frac{d\mathbf{x_p}}{dt} = \mathbf{x_p}, \tag{6}$$

where the velocity of each dispersed particle was governed by Maxey and Riley (1983),

$$\frac{d\mathbf{x_p}}{dt} = -\frac{3}{4}\frac{C_D}{d_p}\left(\frac{\rho_f}{\rho_p}\right)|\mathbf{u_p} - \mathbf{u_f}(\mathbf{x_p})|(\mathbf{u_p} - \mathbf{u_f}(\mathbf{x_p})), \tag{7}$$

where C_D denotes the drag coefficient based on the Stokes force on a sphere with respect to the particle's Reynolds number Re_p,

$$C_D(Re_p) = \frac{24}{Re_p} \quad \text{with } Re_p = \frac{d_p|\mathbf{u_p} - \mathbf{u_f}|}{\nu}. \tag{8}$$

In order to extend the applicability range of Eq. (8) for higher Re_p numbers, an empirical non-linear correction (Clift et al., 1978) was applied, and the drag coefficient was eventually computed from,

$$C_D(Re_p) = \frac{24}{Re_p}\left(1 + 0.15Re_p^{0.687}\right) \tag{9}$$

For high values of Re_p, the drag coefficient reaches a plateau and a constant value is normally adopted for $Re_p > 700$ (Fessler and Eaton, 1999) or $Re_p > 1000$ (Geurts and Vreman, 2006). In the present work, the value of $C_D = 0.43$ was applied for $Re_p > 800$ (Mizuya and Kasagi, 1998) which was well above the values of Re_p computed for all the cases presented in Section 4.

3. Numerical method

An Eulerian approach was adopted for the fluid phase using the fractional step method to solve the set of Navier–Stokes equations (Eq. (3)). Spatial discretization was based on a central finite difference scheme of second order accuracy and time advancement was performed using a fully explicit Adams–Bashforth scheme. A variable time step was computed dynamically according to the convective (*CFL*) and viscous time scale (*VSL*) criteria: $CFL < 0.2$ and $VSL < 0.05$. Details of the numerical scheme and implementation issues can be found in Grigoriadis et al. (2004). The resulting computer code has excellent parallel efficiency, requires 120 Mb of physical memory per million nodes and reaches performances of 0.8 μs/node/iter on personal computers (WinXP, PIV@3.2 GHz).

The core of the numerical methodology was based on the combined application of fast direct pressure solution (Schumann, 1976; Swarztrauber, 1977; Wilhelmson and Ericksen, 1977) and the use of the immersed boundary method (IBM) technique (Balaras, 2004) for the specification of complicated geometries. Instead of using an iterative pressure solution algorithm (like ADI, SOR, Multigrid, etc.), which normally consumes the majority of the total computational effort, a direct pressure solution was adopted. Direct poisson solution is a fast, efficient and parallelizable numerical algorithm for the solution of pressure, but is by nature restricted to orthogonal or cylindrical domains without internal boundaries. That disadvantage was eliminated by the use of the IBM method, which allows the specification of complicated – or even moving – boundaries within rectangular domains with Cartesian grids. The IBM concept is based on the dynamical representation of solid or moving boundaries by mimicking their presence instead of explicitly defining them (Peskin,1972; Mohd-Yusof, 1998; Verzicco et al., 2000). The application of the method in the present work is based on the proper definition of forcing terms in the N–S equations as described in detail in Balaras (2004).

In order to perform the Lagrangian tracking of the dispersed particles, the local fluid velocity $\mathbf{u_f}$ at the particle's location is needed as shown in Eq. (7). Since the particle's location does not coincide with the location of grid nodes and the particle's size can be several orders of magnitude smaller than a typical LES grid cell, an interpolation scheme is normally adopted in order to estimate the local fluid velocity $\mathbf{u_f}(\mathbf{x_p}, t)$. Most of the studies performed so far make use of a combination of high (fourth or even sixth) order Hermite or Lagrange interpolation in homogenous directions and Hermite or Chebychev polynomials in wall normal directions (Armenio et al., 1999; Kuerten, 2006, respectively). In order to minimize the interpolation error introduced in the equation of particle motion, high order interpolation schemes with at least fourth order of accuracy are usually applied in most of the previously reported studies (Kuerten, 2006). However, Marchioli et al. (2007) recently proposed an efficient and accurate interpolation scheme of second order accuracy based on Taylor expansions, which is appropriate for geometrically complicated domains with Cartesian or Curvilinear grids. Using a second order accurate numerical method, considering only the first derivatives and the values of few neighboring nodes (12 instead of 24 used for trilinear interpolation), they demonstrated the simplicity and efficiency of their algorithm for LES in complicated geometries.

In the present study, a similar procedure was used for the estimation of the local fluid velocity $\mathbf{u_f}(\mathbf{x_p}, t)$ which is appropriate for Cartesian flow solvers. Instead of using Taylor expansions, our interpolation method consists of a second order polynomial velocity field reconstruction as shown in Fig. 1. Depending on the location of each particle within a computational cell, the velocities that were taken into account for the interpolation scheme were changed accordingly. The criterion for node selection is that the particle is always contained within the box defined by the closest 12 nodes along the direction of each velocity component. First, the location of eight closest primary velocity locations are identified (full triangles in Fig. 1). Depending on the particle location and the direction considered, the stencil is extended to include another four extra fluid nodes (open arrows in Fig. 1).

Once the interpolation stencil is defined, a total of four velocity field reconstructions are built as piecewise quadratic polynomials along the *x*, *y* or *z* directions, depending on the velocity component. These polynomials evaluate the velocity at the four closest points (marked as *P*1, *P*2 for the plane shown in Fig. 1) which are then used to obtain the fluid velocity by bilinear interpolation. Thus, the interpolation scheme uses only the computed values of velocities at faces, avoiding the interpolation at cell centers which would inevitably lead to smoothing and additional filtering of the solution. Such an effect is definitely undesirable especially in cases where LES computations are performed, as will be discussed later.

One of the main advantages of using such an interpolation scheme, is the fact that the local solution reconstruction can be performed once per time step per cell, and can be easily applied for all the particles contained at the same computational cell. The present method only needs a layer of cells adjacent to the boundaries and can therefore significantly simplify the computation close to external domain boundaries, especially in flow solvers that use fictitious cells around the flow domain (Grigoriadis et al., 2004). In doing so, the demand for special treatment at the boundaries (solid or not) in order to retain the global accuracy of the method is eliminated. Due to the generality of the interpolation scheme, the method can be efficiently and easily implemented within existing Cartesian flow solvers using the IBM method.

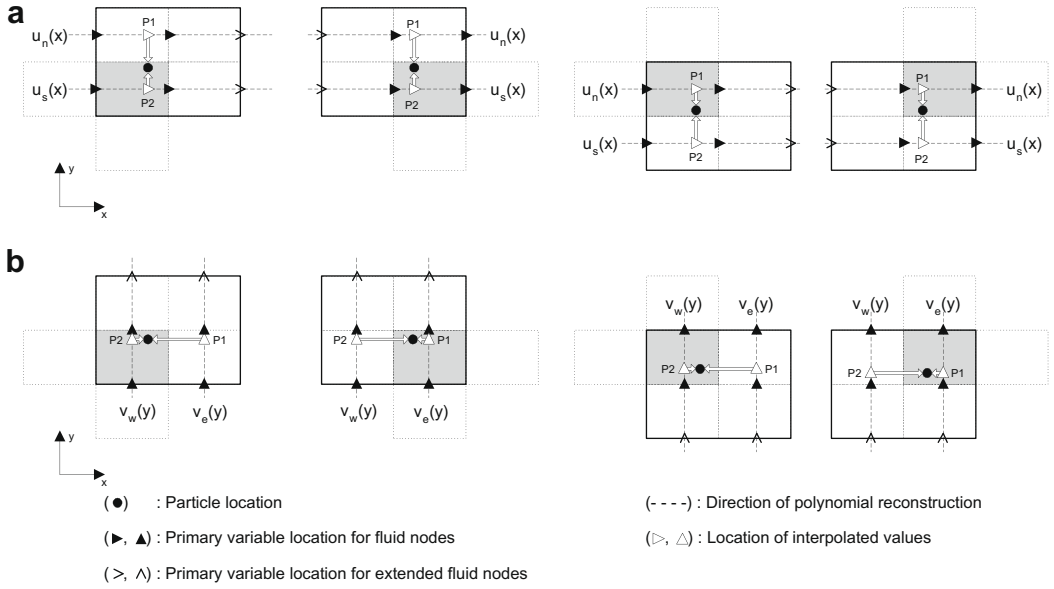

Fig. 1. Interpolation method used for the estimation of the fluid velocity at particle's location in a staggered variable arrangement (shown here for u (a) and v (b) velocity components and performed in a similar fashion for w component). A stencil of the 12 closest nodes to the particle is defined (six nodes are shown here, for one of the two k-planes involved). A piecewise polynomial reconstruction $u_i(j)$ is performed along j direction to define the velocity at the four closest locations (two points P_1 and P_2 are shown here, for one of the two k-planes involved).

The trajectory of each particle was obtained by the time integration of Eq. (6) using a modified Heun's method. Preliminary simulations proved that very similar dispersion results could be obtained even using an Euler scheme for time integration. This fact is due to the fully explicit nature of the numerical algorithm used here and the relatively small time steps taken for time advancement. The use of a higher order integration schemes would thus be justified only in the case of an implicit or a semi-implicit numerical method. The accuracy of the proposed interpolation and integration schemes is demonstrated and verified in the next section where the dispersion results are compared against reference DNS solutions which use high order polynomial interpolations and integration schemes.

4. Results

4.1. Fully developed turbulent channel flow

Simulations of particle-laden fully developed turbulent channel flows were first conducted to validate the numerical algorithm against existing DNS results for a Reynolds number of $Re_\tau = 150$ (Kuerten, 2006).[1] Three different sizes of particles were released with a density ratio $\rho_p/\rho_f = 769.23$ at Stokes numbers $St^+ = 1.0, 5.0, 25.0$ (Table 1). For each case, a total of 100,000 particles were introduced randomly in the flow field with a uniform initial distribution. The computations were performed in a domain with dimensions $4\pi\delta \times 2\pi\delta \times 2\delta$, where δ is the channel's half width, using a numerical resolution of $128 \times 96 \times 90$ cells. Fully elastic collisions were assumed at the walls, and a collision event was recorded every time the distance of the particle from the wall was less than its radius.

In these simulations, the volume fraction for the largest particles shown in Table 1, would imply a two-way coupling between the two phases (Elgobashi, 2006). However, instead of reducing the number of particles by a factor of 44 for this case, it was decided to keep the same number of particles so that a proper statistical sample could be established within a reasonable computational time. Thus, particles were still treated as *transparent*, i.e. the particle motion was not allowed to affect other particles or the carrier flow.

Table 1
Test cases and basic parameters considered for the simulations of particle-laden turbulent channel flow.

Case	Re_τ	$Re_b = \frac{u_b h}{\nu}$	d_p/h	St^+	$\Phi_v \times 10^6$	$\Phi_m \times 10^3$
A	150	2300	1.02×10^{-3}	1.0	0.35	0.27
B	150	2300	2.28×10^{-3}	5.0	3.93	3.02
C	150	2300	5.10×10^{-3}	25.0	43.9	33.8

As the Stokes number increased and heavier particles were dispersed, the near-wall concentration increased significantly while the concentration in the core region reduced. This phenomenon known as *turbophoresis* (Kuerten and Vreman, 2005), can be simply explained by the inertia effects of the heavier particles which are captivated in the slowly-moving near-wall regions as shown in Fig. 2. Fig. 3 shows the predicted rms values of particle velocities for the three different it St numbers considered. In all cases, the agreement with the DNS reference solutions was very good, even for the lower St number cases where no *sgs* model was applied to the local particle velocity.

The tendency to predict increased concentrations close to the walls as Stokes number increases, as well as a slight decrease in the fluctuating components of the particle velocities was verified from all computed cases. These two weak effects are the only ones that differentiate the dispersion pattern between lighter and heavier particles in a turbulent channel flow. Overall, the dispersion pattern and the associated statistics showed a qualitatively similar behavior for different particle sizes.

4.2. Particle dispersion over a two-dimensional obstacle

The present case considered line-injection of a passive scalar inside the wake of a wall mounted two-dimensional square obstacle, according to the experimental study of Vincont et al. (2000). The Re_h number based on the obstacle's dimension h and the free

[1] Available at http://cfd.cineca.it/cfd/repository/ (Marchioli et al., 2008).

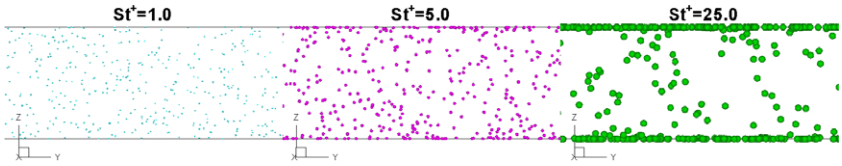

Fig. 2. Instantaneous dispersion patterns in a fully developed turbulent channel for various St^+ numbers at $Re_\tau = 150$. The flow is directed inwards, walls are perpendicular to z-direction, particles are magnified 1000 times and 0.5% of the total number of particles is shown.

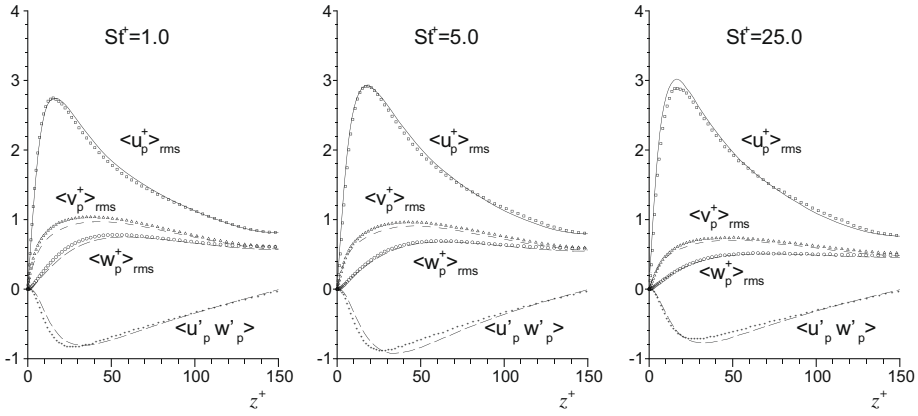

Fig. 3. Predicted fluctuating components of particle velocity in a fully developed turbulent channel for various St^+ numbers at $Re_\tau = 150$. (Symbols): DNS by Kuerten (2006), (lines): present LES computations.

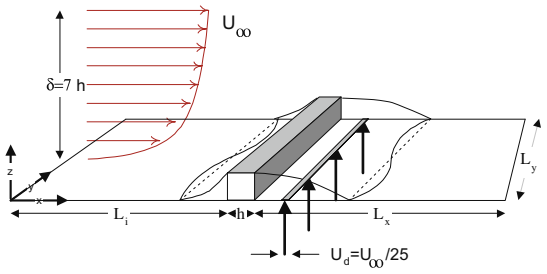

Fig. 4. Coordinate system and computational domain used for the dispersion in the wake of a two-dimensional obstacle. Particles are injected from a slot with a width of $d = 0.7\,h$ with an initial velocity of $U_d = 4\%U_\infty$.

stream velocity U_∞ was 740 while the oncoming BL had a thickness of $\delta = 7h$. A passive scalar was injected normally through a slot of width $h/7$ at a distance h after the body, with an injection speed of $U_d/U_\infty = 4\%$, as shown in Fig. 4. The existence of the obstacle was prescribed using the immersed boundary method.

LES calculations were performed on a computational domain with dimensions $(L_i + L_x, L_y, L_z) = (5\delta_{inl} + 4\delta_{inl}, 3\delta_{inl}, 3\delta_{inl})$. An inlet generation procedure based on boundary layer rescaling has been applied to provide a realistic inflow condition for the simulation (Grigoriadis, 2006). Two different numerical resolutions have been used with $192 \times 48 \times 64$ or $320 \times 48 \times 130$ cells, using both an Eulerian and a Lagrangian approach for the dispersed phase. All the calculations performed in the present section were conducted using the filtered structure function model (FSF hereafter) of Ducros et al. (1996), unless otherwise stated. The simulations were performed for a total time of $\approx 550h/U_\infty$ and a total of 40,000 statistical samples were collected for the flow field and the particles during the time interval $t = 350{-}550h/U_\infty$.

For the limiting case of $St = 0$, particles tend to disperse in a more uniform manner and particle trajectories coincide with fluid trajectories. Due to the lack of any inertia effects, these particles do instantaneously adjust to the local flow conditions by following every single vortical motion created by the flow field. Therefore, in such a limiting case one can directly compare the results of a typical Eulerian approach using a turbulent diffusivity for the dispersed phase. Such a comparison was performed in the present study by performing two different simulations to verify the methodology. In the first Eulerian calculation, the dispersed phase was governed by the solution of a transport equation for concentration with a Schmidt number of $Sc = 2500$ in accordance with the experimental study of Vincent et al. (2000). A turbulent Schmidt number of $Sc_t = 0.6$ was used to estimate the turbulent diffusivity.

For the second set of Lagrangian simulations, the equation of motion for each solid particle was solved, and the concentration field was estimated from the predicted trajectories of each particle. In order to ensure similarity, the particles were injected in a random fashion from the slot, with an initial velocity of $0.04U_\infty$. A total of 200,000 solid, spherical particles were injected for each St number, with a density ratio $\rho_p/\rho_f = 769.23$. The concentration field was normalized with respect to the predicted concentration value C_s over the slot.

Fig. 5b, shows the comparison between these two simulations for the time-averaged concentration field C/C_s using the coarser numerical resolution of $192 \times 48 \times 64$ cells. In that case, the Lagrangian simulation underestimated the dispersion especially in the primary recirculation region. This effect is due to the insufficient resolution of the flow field which is crucial for smaller St numbers when a sgs model is not used for the particle velocity. When the finer numerical resolution of $320 \times 48 \times 130$ cells was used (Fig. 5c), a very satisfactory agreement was reached between the two approaches, which verifies the Lagrangian tracking methodology used in the present study. The adequacy of numerical resolution for the finer grid was also supported by the fact that when the Smagorinsky model was used, minor changes in the predicted dispersion pattern were noticed.

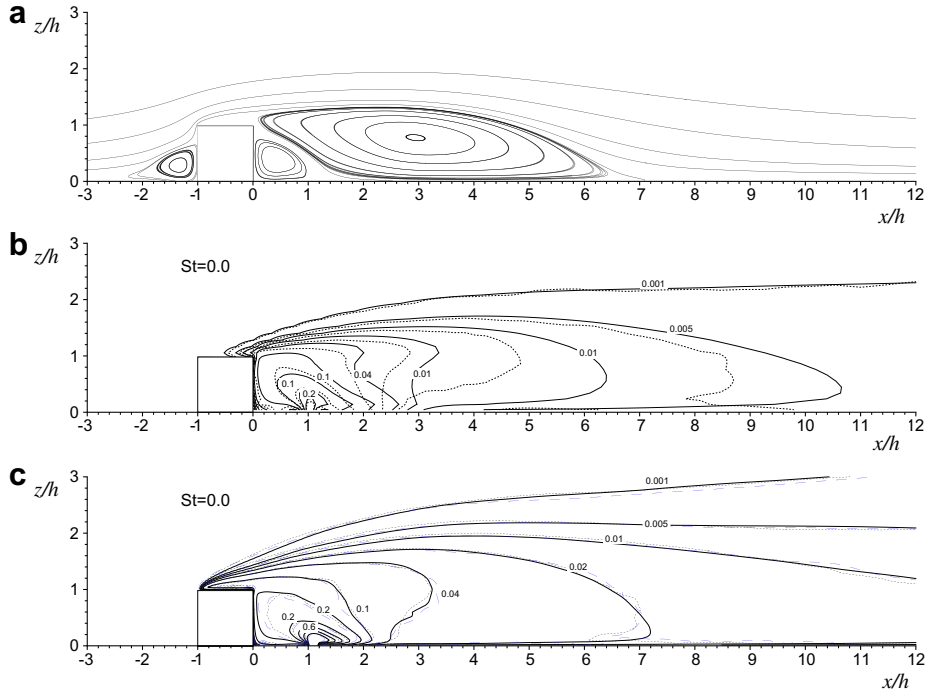

Fig. 5. Mean velocity field and time-averaged concentration fields C/C_s of inertialess particles ($St = 0$) in the wake of a wall-mounted obstacle using the Eulerian (solid lines) and the Lagrangian approaches (dashed lines). (a) Mean velocity streamlines, (b) coarse numerical resolution of $192 \times 48 \times 64$ cells, (c) fine numerical resolution of $320 \times 48 \times 130$ cells. (- - - -): Lagrangian simulations with the Filtered structure function model, $(\cdots)$: Lagrangian simulations using the Smagorinsky turbulence model with $C_s = 0.1$.

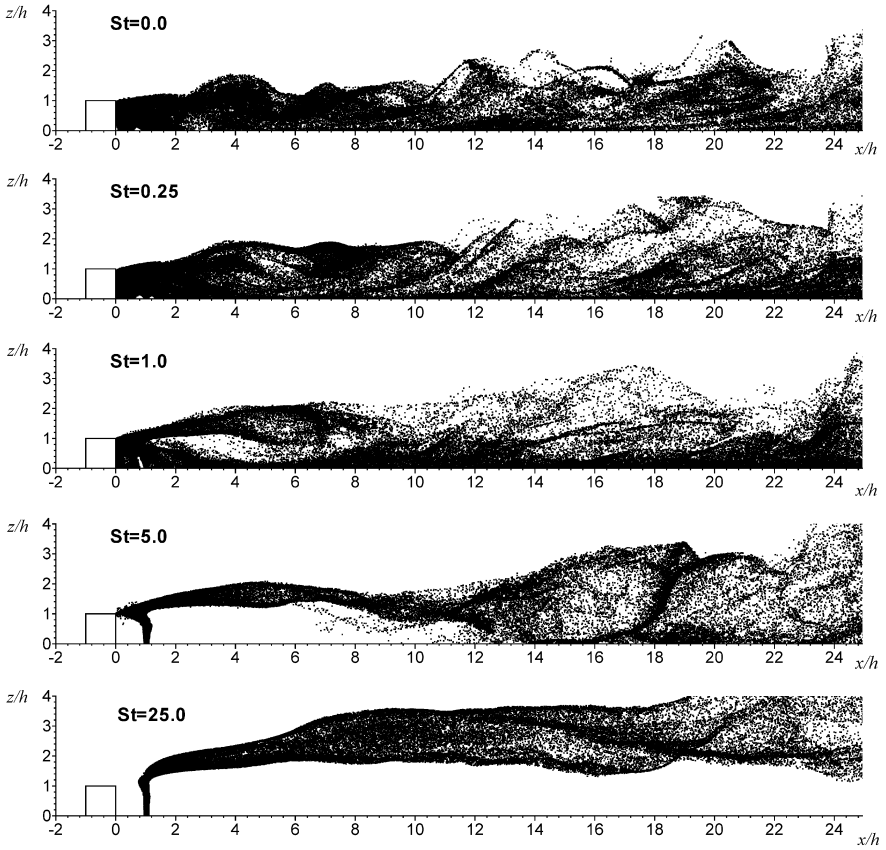

Fig. 6. Effect of particle size on snapshots of the instantaneous concentration fields (particles of different *St* number are plotted as points of the same size).

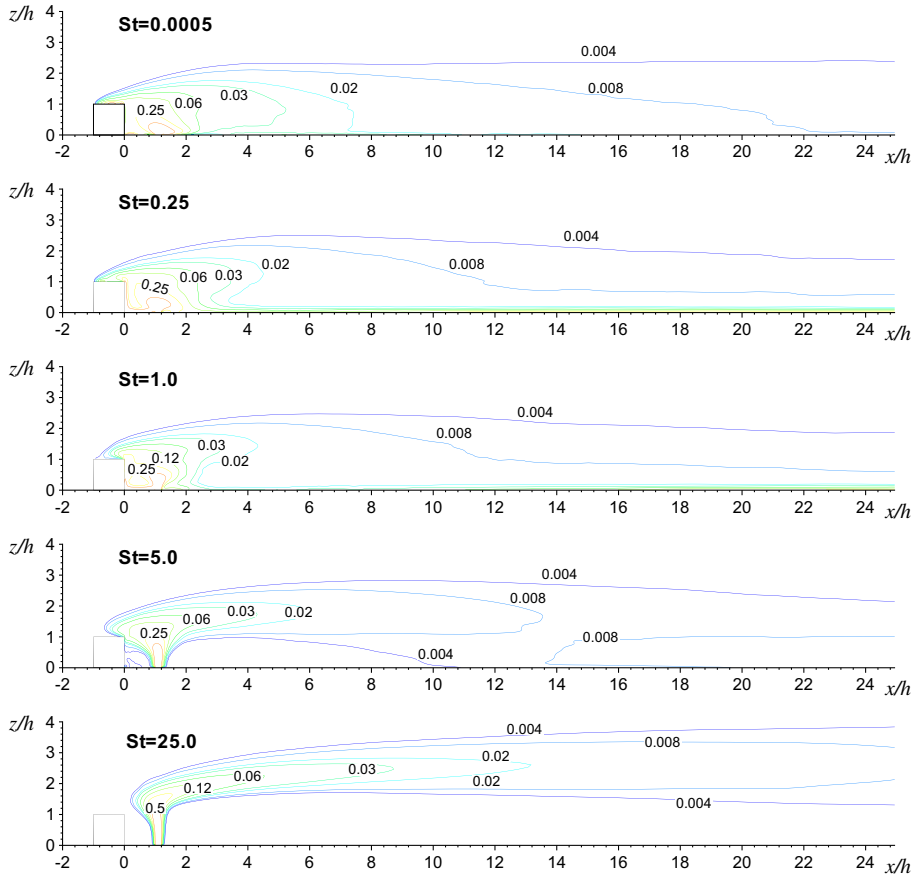

Fig. 7. Effect of particle size on the time averaged concentration field C/C_s.

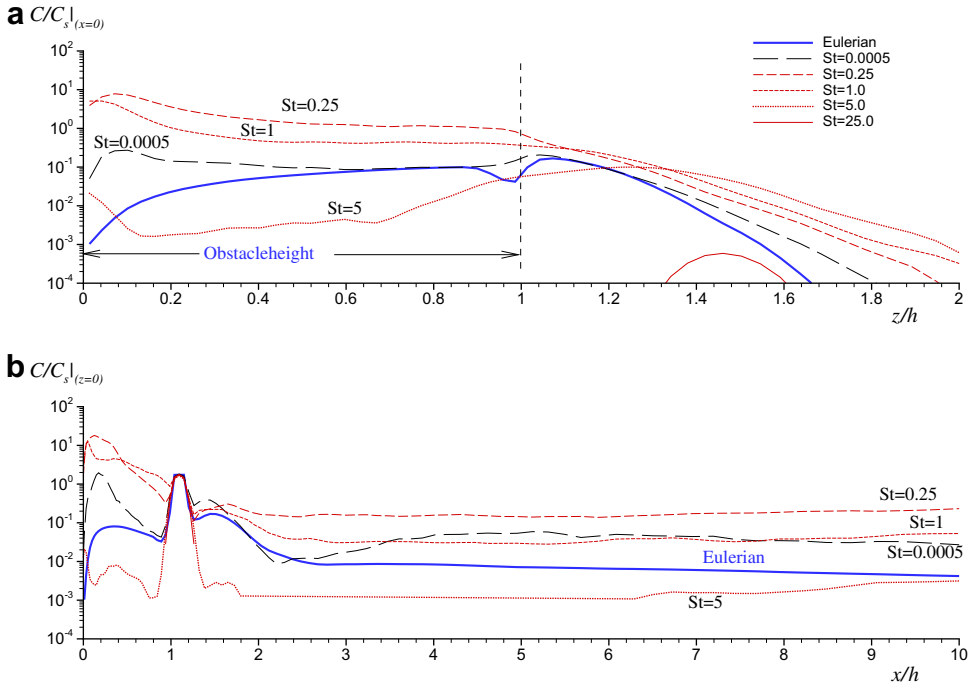

Fig. 8. Particle accumulation along the downstream facing wall of the obstacle (a), and the lower wall (b). The time-averaged mean concentration C/C_s is plotted within a strip of thickness $0.02h$ away from the walls.

Some weak fluctuations observed at the end of the wake for Lagrangian calculations using the finer grid (Fig. 5c), are due to the highly intermittent character of the flow and the sampling procedure adopted for the concentration statistics. The statistical *window* at each location coincided with the local size of the control volume as defined by the non-uniform grid used. A statistical

sample was taken every time a particle was tracked inside a control volume. Therefore, depending on the numerical resolution, the population and the motion of the particles, eventually a different number of samples may be collected at each grid location. Thus for Lagrangian inhomogeneous cases like the one considered, the particle statistics may still look intermittent when compared to Eulerian simulation, especially at higher numerical resolutions in regions of high unsteadiness such as the reattachment region. Although increasing the number of released particles over 200,000, the sampling period over $t = 200h/U_\infty$ and/or the number of collected samples over 40,000 would be definitely desirable, it would significantly increase the computational cost.

The strong effect of particle size on the instantaneous dispersion characteristics is demonstrated in Fig. 6 where a snapshot of the particle location is shown for different *St* numbers. As expected, for the lower *St* number cases, particle motion is more sensitive to the local flow field. In these cases, light particles are captured by the primary and secondary recirculation regions (Fig. 5a) and travel upstream towards the obstacle before they are convected by the oncoming turbulent stream. For larger *St* numbers though, the dispersion pattern differs significantly because these particles tend to ignore the surrounding recirculation patterns. Since the heavier particles possess sufficient initial inertia to escape from the obstacle's wake, they are almost directly injected into the shear layer generated by the obstacle.

This is also demonstrated in Fig. 7, which presents the time averaged concentration field. As *St* number increases, the core of the plume moves higher, and for the higher *St* numbers, a chimney-like dispersion pattern is produced. Even if gravity force was included in the equation of particle's motion, their trajectories would not be significantly affected close the injection point due to their large initial inertia. Further downstream though, the effect of gravity would gradually 'bend' the generated plume towards the lower wall as demonstrated in previous studies of particle dispersion (Yua et al., 2004). Thus, the inclusion of gravity effects would be expected to delay the transition to a chimney-like dispersion pattern and lead to enhanced particle accumulation at the lower wall away from the obstacle.

Wall concentration and regions with particle accumulation were also found to heavily depend on the *St* number. Due to the interaction of the particles with the wake, the concentration at the obstacle's upper wall was found to reduce with *St* number. As shown in Fig. 7, the region with maximum concentration is wider and it is located between the slot and the obstacle for the lower *St* numbers. For higher values of *St*, it becomes narrower and tends to align along the direction of the particle's initial velocity.

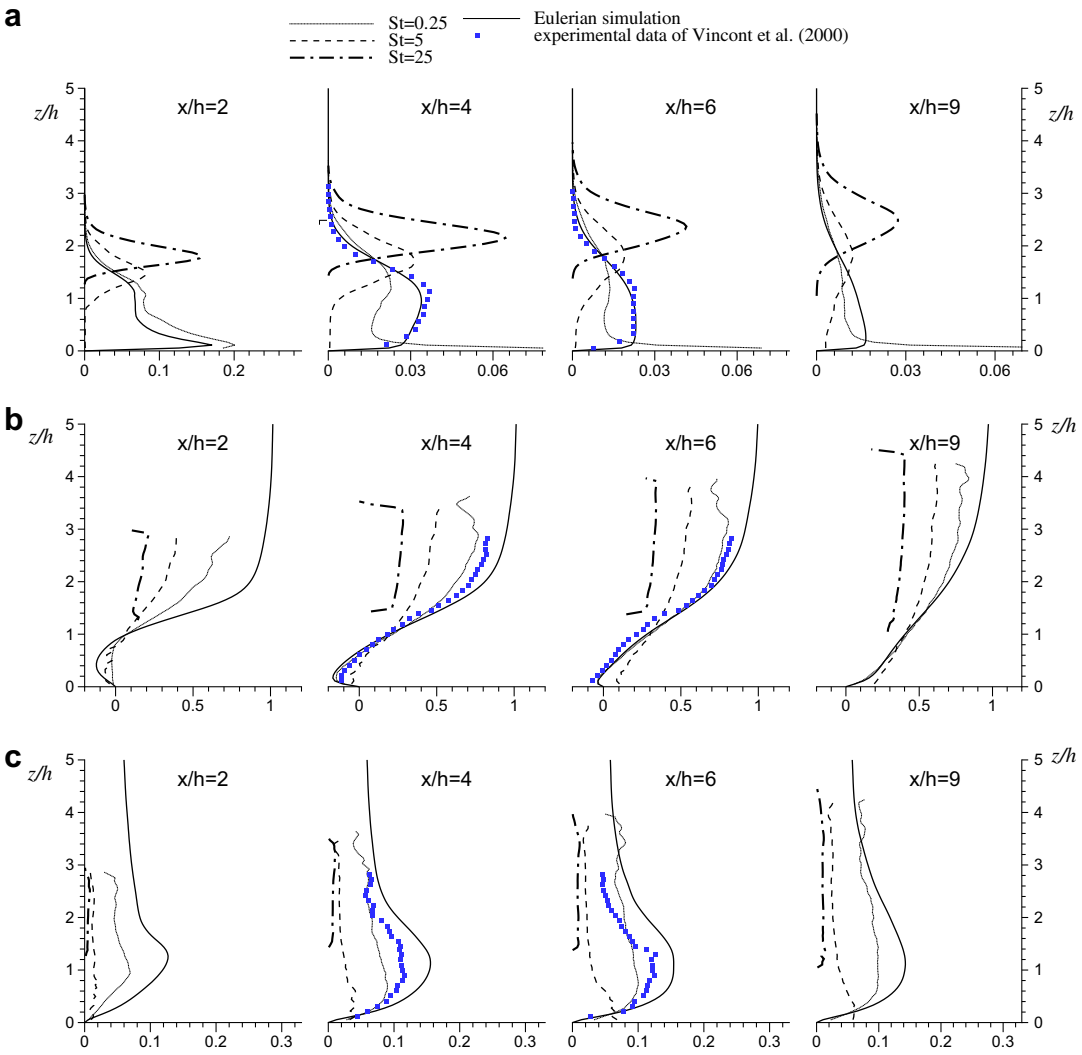

Fig. 9. Vertical distribution of mean properties in the wake region against the experimental data of Vincont et al., 2000. (a) Mean concentration C/C_s, (b) mean streamwise velocity u/U_∞, (c) fluctuating component of the vertical velocity component w_{rms}/U_∞.

Fig. 8a and b present the mean wall concentrations along the downstream facing wall ($x = 0$–$0.02h$) and the lower wall ($z = 0$–$0.02h$), respectively. For very light particles the concentration along the obstacle wall was close to the value of $C/C_s \approx 0.1$, while the higher particle-concentration was found for intermediate particles with $St \approx 0.25$ which accumulate at the corner. As St increases, heavier particles gradually avoid the secondary recirculation leading to lower concentrations along the obstacle's wall. For $St = 25$, the obstacle's wall was found completely free of particles.

This non-monotonic behavior was also apparent if one examines the concentration along the lower wall after the obstacle (Fig. 8b) and resembles preferential concentration effects in flows like mixing layers (Eaton and Fessler, 1994). The overall accumulation at the lower wall was maximum for $St = 0.25$, and was also found to reduce for $St > 0.25$. Particle accumulation was maximum at $x/h \approx 0.1$, decayed fast before reaching the slot, while lower particle accumulation gradients were observed further downstream.

This tendency for preferential concentration in the lower wall after the obstacle is also evident from Fig. 9a. For example, when particles with $St = 0.25$ are dispersed, most of the particles are accumulated in the lower wall region. Further downstream, heavier particles gradually escape from the recirculation region and a Gaussian-type dispersion was found for $St > 1$. The velocity of the particles was also significantly affected by particle size as shown in Fig. 9b and c. The slip velocity of the particles increased monotonically with the St number downstream of the obstacle. Due to their larger inertia, heavier particles were therefore found to move slower with velocities as low as 50% with respect to the fluid particles at distances as far as $10h$ after the obstacle. Additionally, as shown in Fig. 9c, for very heavy particles smooth velocity profiles were predicted with very small fluctuations. Such a uniformity implies that the majority of heavier particles tend to travel with similar and nearly constant in time velocity at each location.

5. Conclusions

Large-eddy simulations of particle-laden flows in homogeneous and inhomogeneous turbulent flows were presented. A Lagrangian particle tracking algorithm was used for the simulation of the dispersed phase, based on a simple local reconstruction of the flow field at the particle's location. Such a method was found to be well suited and accurate for dispersion studies in turbulent flows using the IBM for the specification of complicated geometries.

The effect of several modelling parameters was analyzed and comparisons with an Eulerian description of the dispersed phase was also performed. Analysis of the computed cases verified the strong effect of particle size and inertia on the dispersion pattern, especially for the inhomogeneous case considered where particles were injected inside the wake of an obstacle. In these cases, the produced dispersion pattern and the associated statistics showed a much stronger dependence on the St number. Preferential concentration effects in the near-wall regions were identified only for an intermediate range of St numbers. For higher St number, Gaussian-like dispersion patterns were predicted after the obstacle. The effect of insufficient grid resolution was found to reduce the dispersion of particles. The extension to cases with two-way or four-way coupling between the two phases is under progress.

Acknowledgements

This work has been performed under the UCY-CompSci project, a Marie Curie Transfer of Knowledge (TOK-DEV) Grant (Contract No. MTKD-CT-2004-014199) funded by the CEC under the 6th Framework Program. Partial support by a Center of Excellence grant from the Norwegian Research Council to Center for Biomedical Computing is also greatly acknowledged.

References

Armenio, V., Fiorotto, V., 2001. The importance of the forces acting on particles in turbulent flows. Phys. Fluids 13 (8), 2437.
Armenio, V., Piomelli, U., Fiorotto, V., 1999. Effect of the subgrid scales on particle motion. Phys. Fluids 11 (10), 3030.
Arcen, B., Taniere, A., Oesterle, B., 2006. On the influence of near-wall forces in particle-laden channel flows. Int. J. Multiphase Flow 32 (12), 1326–1339.
Balaras, E., 2004. Modeling complex boundaries using an external force field on fixed Cartesian grids in large-eddy simulations. Comput. Fluids 33, 375–404.
Clift, R., Grace, J.R., Weber, M.E., 1978. Bubbles, Drops and Particles. Academic Press, New York.
Ducros, F.D., Comte, P.C., Lesieur, M., 1996. Large-eddy simulation of transition to turbulence in a boundary layer developing spatially over a flat plate. J. Fluid Mech. 326, 1–36.
Eaton, J.K., Fessler, J.R., 1994. Preferential concentration of particles by turbulence. Int. J. Multiphase Flow 20, 169–209.
Fessler, J.R., Eaton, J.K., 1999. Turbulence modification by particles in a backward-facing step flow. J. Fluid Mech. 394, 97–117.
Elgobashi, S., 2006. An updated classification map of particle-laden turbulent flows. In: Balachandar, S., Prosperetti, A. (Eds.), Proceedings of the IUTAM Symposium on Computational Multiphase Flow. Springer.
Geurts, B.J., Vreman, B., 2006. Dynamic self-organization in particle-laden channel flow. Int. J. Heat Fluid Flow 27, 945–954.
Grigoriadis, D.G.E., 2006. Large-eddy simulations of spatially developing flows using inlet conditions. In: Direct and Large-Eddy Simulation VI, Proceedings of the Sixth International ERCOFTAC Workshop on Direct and Large-Eddy Simulation, ISBN: 1-4020-4909-9.
Grigoriadis, D.G.E., Bartzis, J.G., Goulas, A., 2004. Efficient treatment of complex geometries for large-eddy simulations of turbulent flows. Comput. Fluids 33 (2), 201–222.
Kuerten, J.G.M., 2006. Subgrid modeling in particle-laden channel flow. Phys. Fluids 18, 025108.
Kuerten, J.G.M., Vreman, A.W., 2005. Can turbophoresis be predicted by large-eddy simulation? Phys. Fluids 17 (1), 011701.
Li, X.-X., Liu, C.-H., Leung, D.Y.C., Lam, K.M., 2006. Recent progress in CFD modelling of wind field and pollutant transport in street canyons. Atmos. Environ. 40, 5640–5658.
Marchioli, C., Armenio, V., Soldati, A., 2007. Simple and accurate scheme for fluid velocity interpolation for Eulerian–Lagrangian computation of dispersed flows in 3D curvilinear grids. Comput. Fluids 36, 1187–1198.
Marchioli, C., Picciotto, M., Soldati, A., 2007. Influence of gravity and lift on particle velocity statistics and transfer rates in turbulent vertical channel flow. Int. J. Multiphase Flow 33 (3), 227–251.
Marchioli, C., Armenio, V., Soldati, A., Salvetti, M.V., 2006. Mechanisms for deposition and resuspension of heavy particles in turbulent flow over wavy interfaces. Phys. Fluids 18, 025102.
Marchioli, C., Soldati, A., Kuerten, J.G.M., Arcen, B., Taniere, A., Goldensoph, G., Squires, K.D., Cargnelutti, M.F., Portela, L.M., 2008. Statistics of particle dispersion in Direct Numerical Simulations of wall-bounded turbulence: results of an international collaborative benchmark test. Int. J. Multiphase Flow 34 (9), 879–893.
Maxey, M.R., Riley, J.J., 1983. Equation of motion for a small rigid sphere in a nonuniform flow. Phys. Fluids 26, 883.
Mizuya, T., Kasagi, N., 1998. Numerical analysis of particle motion in turbulent channel flow. In: Proc. Third Int. Conf. Multiphase Flow, Lyon, June 1998.
Mohd-Yusof, J., 1998. Development of immersed boundary methods for complex geometries CTR. In: Proceedings of the Summer Program, Stanford University, pp. 325–335.
Peskin, C.S., 1972. Flow patterns around heart valves: a numerical method. J. Comput. Phys. 10, 252–271.
Schumann, U., 1976. A direct method for the solution of Poisson's equation with Neumann boundary conditions on a staggered grid of arbitrary size. J. Comput. Phys. 20, 171–182.
Swarztrauber, P.N., 1977. The methods of cyclic reduction, Fourier analysis and the FACR algorithm for the discrete solution of Poisson's equation on a rectangle. J. Comput. Phys. 19 (3), 490–501.
Verzicco, R., Orlandi, P., Mohd-Yusof, J., Haworth, D., 2000. LES in complex geometries using boundary body forces. AIAA J. 38 (3), 427–433.
Vincont, J.Y., Simoens, S., Ayrault, M., Wallace, J.M., 2000. Passive scalar dispersion in a turbulent boundary layer from a line source at the wall and downstream of an obstacle. J. Fluid Mech. 424, 127–167.
Yua, K.F., Lau, K.S., Chan, C.K., 2004. Numerical simulation of gas-particle flow in a single-side backward-facing step flow. J. Comput. Appl. Math. 163, 319–331.
Wang, Q., Squires, K., Chen, M., McLaughlin, J., 1997. On the role of lift force in turbulence simulations of particle deposition. Int. J. Multiphase Flow 23, 749–763.
Wilhelmson, R.B., Ericksen, J.H., 1977. Direct solutions for Poisson's equation in three dimensions. J. Comput. Phys. 25, 319–331.